ELSEVIER

Materials Science and Engineering C 23 (2003) 129–140

MATERIALS SCIENCE & ENGINEERING C

www.elsevier.com/locate/msec

Nanowires and nanotubes

M.S. Dresselhaus[a,b,*], Y.M. Lin[b], O. Rabin[c], A. Jorio[a,d], A.G. Souza Filho[a,e], M.A. Pimenta[d], R. Saito[f], Ge.G. Samsonidze[b], G. Dresselhaus[g]

[a] *Department of Physics, Massachusetts Institute of Technology (MIT), Cambridge, MA 02139-4307, USA*
[b] *Department of Electrical Engineering and Computer Science, MIT, Cambridge, MA 02139-4307, USA*
[c] *Department of Chemistry, MIT, Cambridge, MA 02139-4307, USA*
[d] *Departamento de Física, Universidade Federal de Minas Gerais, Belo Horizonte, Minas Gerais 30123-970, Brazil*
[e] *Departamento de Física, Universidade Federal do Ceará, Fortaleza, Ceará 60455-760, Brazil*
[f] *Department of Electronic Engineering, University of Electro-Communications and CREST, JST, Tokyo 182-8585, Japan*
[g] *Francis Bitter Magnet Laboratory, MIT, Cambridge, MA 02139-4307, USA*

Abstract

Nanowires and nanotubes are now at the forefront of materials science at the nanoscale. This article starts with introductory comments about nanowires and nanotubes and then addresses in more detail the special structure and properties of bismuth nanowires and carbon nanotubes, which are considered as prototype examples of nanowires and nanotubes. Both nano-materials are important for the new nanoscience concepts that they introduce and for their promise for practical applications. Both provide a system that is simple enough so that detailed calculations of their properties can be carried out, and predictions about their physical behavior can be made. The occurrence and control of unusual and unique properties of specific nanostructures are the drivers for the exploitation of nanoscience in nanotechnology applications.

Keywords: Nanowires; Nanotubes; Nanoscience

1. Introduction

Within the realm of nanoscience and nanotechnology, nanowires and nanotubes play a special role because of their one-dimensionality. When the nanowire or nanotube diameter becomes small, singularities in the electronic density of states develop at special energies, called van Hove singularities, where the electronic density of states becomes very large (see Fig. 1), resembling more closely the case of molecules and atoms, but appearing to be very different from the case of crystalline solids or even two-dimensional systems. Thus, in the limit of small diameters, such as pertaining to bismuth nanowires or single wall carbon nanotubes, which are emphasized in this article, novel quantum phenomena associated with this characteristic 1-D density of states features are observed. In general, a long thin nanowire [1] or a single wall nanotube, consisting of a single atomic layer shell [2], is expected to show pronounced quantum effects in the limit of small diameters.

The occurrence of nanotubes is normally associated with layered bulk materials, such as graphite [2], BN [3], or transition metal dichalcogenides (MoS_2 and WS_2) [3–6], which have strong in-plane forces within the layer plane, but weak interplanar (interlayer) van der Waals forces. More isotropic materials, such as Si [7], III–V and II–VI semiconducting compounds [8,9], oxides such as SiO_2 or In_2O_3, IV–VI compounds such as PbTe [7,10,11], and metals such as Ni [12,13], Co [13,14], all tend to form nanowires.

It is particularly interesting to note that some materials, such as bismuth, can exhibit a variety of different 1-D nanostructures, such as nanowires [1], nanotubes [15], and nanolines [16], as shown schematically in Fig. 2. Since Bi nanowires down to 7 nm diameter maintain the same basic rhombohedral lattice structure with the same values of the lattice constants as bulk bismuth, it is possible to make many detailed predictions about the electronic properties of

* Corresponding author. Department of Electrical Engineering and Computer Science, Massachusetts Institute of Technology, 77 Massachusetts Ave. Room 13-3005, Cambridge, MA 02139-4307, USA. Tel.: +1-617-253-6864; fax: +1-617-253-6827.
E-mail address: millie@mgm.mit.edu (M.S. Dresselhaus).

0928-4931/02/$ - see front matter © 2002 Elsevier Science B.V. All rights reserved.
PII: S0928-4931(02)00240-0

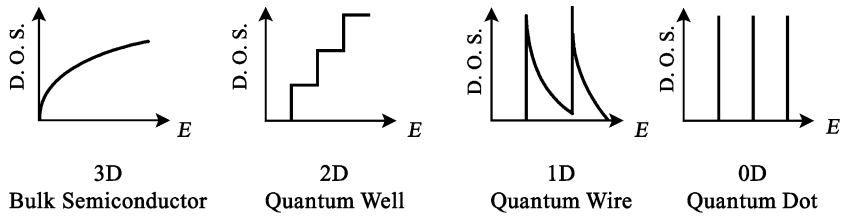

Fig. 1. Electronic density of states for (a) bulk 3-D crystalline semiconductor, (b) 2-D quantum well, (c) 1-D nanowire or nanotube and (d) 0-D quantum dot.

bismuth nanowires based on the bulk properties of bismuth [1], and good agreement between predictions and experimental observations is obtained.

For the case of bismuth nanotubes (see Fig. 3), neither the structure nor the physical properties are well established at this time. Early reports of X-ray diffraction measurements suggest that the structure of single-walled bismuth nanotubes appears to contain a single layer of the basic rhombohedral structural unit of bulk bismuth, containing two atoms per unit cell with the same space group and almost the same lattice constants as bulk bismuth [15]. In this case, the properties of bismuth nanotubes would be expected to bear some resemblance to those of crystalline bismuth, insofar as they have common unit cells, though distinctly different detailed behaviors would also be expected, reflecting the different structural environments of these unit cells within the two systems. Future experiments and calculations on Bi nanotubes will be very interesting in illuminating these relations.

Finally, we have a third type of one-dimensional structure for bismuth, namely the bismuth nanolines shown schematically in Fig. 2c, consisting of two atom-wide bismuth lines embedded within the surface layer of a silicon crystal (see inset to Fig. 4), obtained by the substitution of two bismuth atoms for three Si atoms in the silicon surface lattice structure, with the bismuth nanolines oriented along the $1\bar{1}0$ direction [16]. Such a self-assembly process works because Bi acts as a surfactant in Si. Since two Bi atoms are insufficient to establish a periodic potential resembling that of bulk bismuth, the electronic structure of Bi nanolines is expected to be very different from that of their Bi nanowire or nanotube counterparts. Detailed calculations based on a different potential function would be necessary to establish the electronic structure of a bismuth nanoline although each bismuth atom has the same potential in the atomic limit. Bismuth nanolines have attracted interest because of their very straight line structure (see Fig. 4), their ability to self assemble and to grow from a nucleation site in the silicon surface layer, and their metallic electronic properties, thereby suggesting possible future applications for nano-connections in nano-electronic devices. In the context of nanoscience, we see that a given elemental solid, such as bismuth, can exhibit a number of different nanostructures, implying that each has very different physical properties. Such possibilities offer exciting opportunities for the discovery of new scientific principles and applications.

From a technology standpoint, great progress has been made by showing that it is possible to synthesize a large number of highly crystalline semiconducting nanowires [10,18,19], and when the nanowire diameters are small enough, lasing action can be observed [20,21]. The availability of nanowire lasers, such as the ZnO laser shown in Fig. 5, will be important for the development of the nano-opto-electronics field. By varying the diameter of the nanowire for a given semiconducting material, the lasing frequency can be controlled. In addition, band gap engineering based on the selection of the semiconducting material (e.g., GaAs or GaP) provides another method for controlling the laser frequency, which can further be fine-tuned by alloying one semiconductor with another (e.g., $GaAs_{1-x}P_x$). Thus, lasing nanowires offer many possibilities for nanoscale opto-electronic devices, where individual heterojunctions could be addressed by an optical gate.

A further breakthrough was recently provided by the demonstration of segmented nanowires or an array of periodic nanowire heterojunctions (see Fig. 6) [22–24]. In the context of semiconducting nanoelectronic devices, a

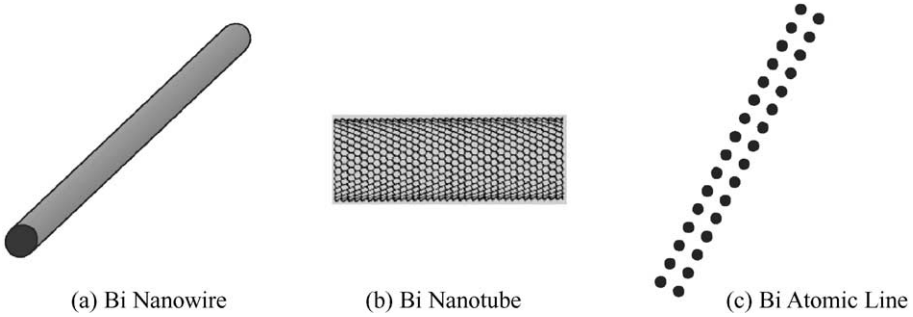

Fig. 2. Various nano-structural forms of elemental bismuth that have been achieved experimentally, including (a) a Bi nanowire, (b) a Bi nanotube, and (c) a Bi nanoline consisting of two adjacent bismuth atoms along a $(1\bar{1}0)$ direction on a Si surface.

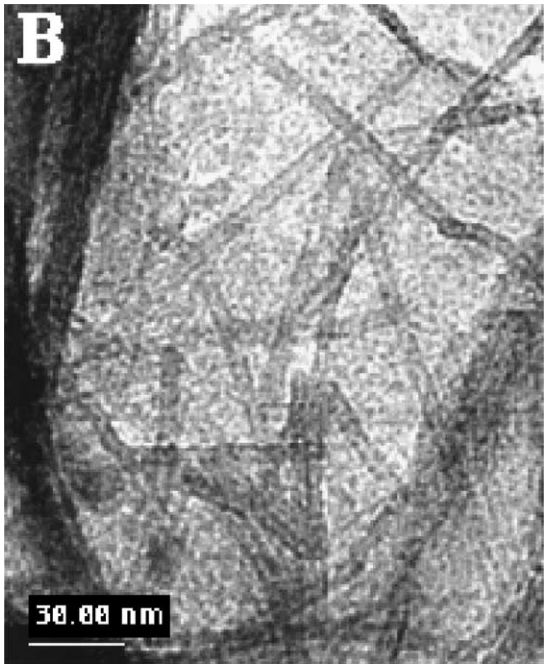

Fig. 3. A transmission electron microscope image of bismuth nanotubes. The X-ray diffraction pattern shows that bismuth nanotubes have the same space group $R\bar{3}m$(166) as bulk bismuth with similar lattice constants [15].

segmented nanowire can be viewed as a superlattice of quantum wells and barriers, where each well-barrier junction could in some way be addressed, as for example by a semiconducting sleeve that could be used as a gate and might be self-assembled or fabricated around the junction between the quantum well and barrier. In the context of thermoelectricity applications, such a segmented nanowire

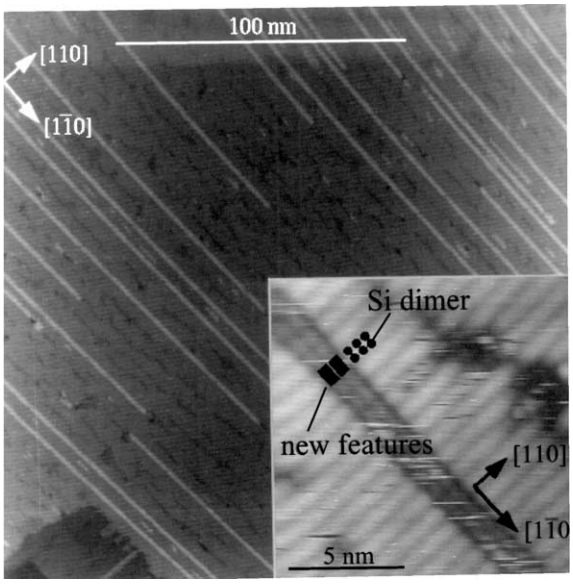

Fig. 4. Bismuth nanolines formed by the exposure of a clean Si surface to Bi below its desorption temperature, followed by annealing close to the desorption temperature. The inset is a close-up (12.9×12.9 nm^2) STM image of Bi nanolines in a silicon surface layer [16].

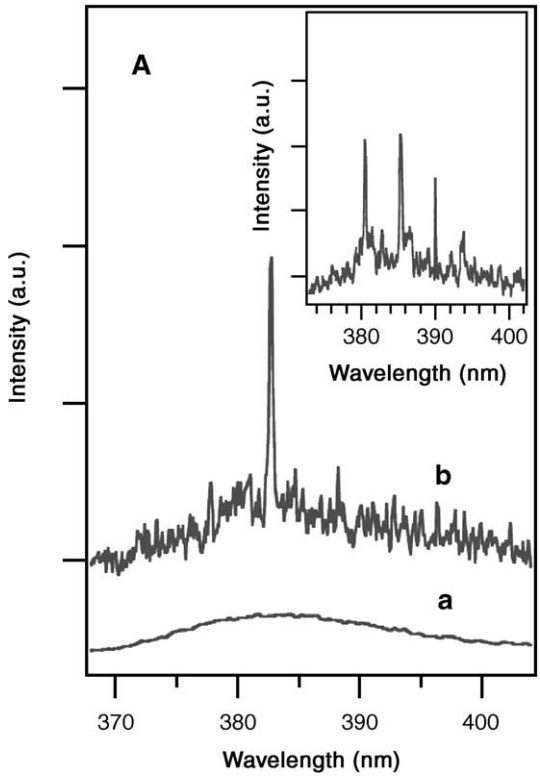

Fig. 5. Emission spectra for ZnO nanowire arrays below (line a) and above (line b) the lasing threshold. The inset shows various lasing modes for the ZnO nanowire cavity [17].

might be constructed of isoelectronic materials (such as Bi_2Te_3 and Bi_2Se_3) that permit easy electron transport along the nanowire, but strongly inhibit phonon transport by enhanced phonon scattering at each interface because of a large difference in atomic mass between the chemical constituents at the two sides of the interface [25,26].

At this early stage of studying nanowires and nanotubes, it would appear useful to look for distinctive aspects within

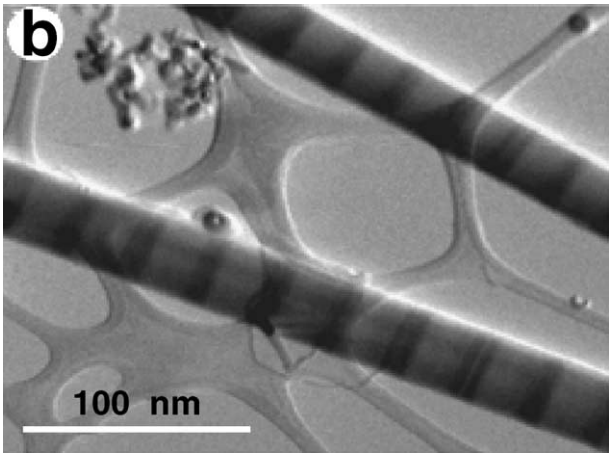

Fig. 6. STEM image of two Si/SiGe segmented nanowires. The darker regions represent SiGe segments while the lighter regions represent Si segments. The background shows a holey carbon net used for TEM observations [22].

these structures. If we view nanotubes as being formed by the rolling up of a strongly bonded layer that is weakly coupled to the external world, we can envisage the external surface of the nanotube as weakly interacting from a chemical standpoint, requiring little passivation when eventually used for electronic devices. In contrast, a semiconducting nanowire grown along the (100), (110), or (111) directions will exhibit many dangling bonds at the interface. For some applications, which might benefit from bonding to the nanowire, such dangling bonds might be desirable, while for other applications requiring chemical stability of the interface, passivation of the surface is necessary. Depending on the intended application, the dangling bonds at the exposed surface of semiconducting nanowires could, if it were a silicon nanowire, be passivated by oxide formation or by hydrogen termination. The very much smaller concentration of dangling bonds on the exposed surface of a carbon nanotube substantially simplifies the passivation problem in device applications based on carbon nanotubes, even though care must be taken to control the amount and nature of the adsorbed gases, if these adsorbed gas molecules should affect device performance. Adsorbed gases, on the other hand, could be useful for applications of carbon nanotubes as a gas sensor, or for *p*-type doping of carbon nanotubes by adsorbed oxygen.

Many of the unique properties of carbon nanotubes arise because of the linear E vs. k relations at the Fermi level of 2-D graphite, rather than the parabolic $E(k)$ relation commonly found in semiconductors. This unique linear k behavior is responsible for many unique electronic and vibrational properties of 2-D graphite and of their related carbon nanotubes. One of the unique properties that follow from these special dispersion relations is the possibility of metallic or semiconducting nanotubes, depending on the nanotube geometry. While carbon nanotubes offer this amazing flexibility in electronic properties, the *control* of their geometry during synthesis, or the external control of the metallic vs. semiconducting properties of a nanotube by external perturbations, still remains illusive. In contrast, BN nanotubes are always insulating (or semiconducting), independent of diameter and chirality.

Nanowires and nanotubes are complementary materials, each having novel and remarkable properties; many of which are now being explored for the first time. It is hoped that some of these novel and remarkable properties will someday be exploited in important nanotechnology applications. In this article, we focus on two examples of new physics provided by nanowire and nanotube structures, namely the semimetal–semiconductor transition and recent progress with observations of this effect in bismuth nanowires (Section 2), and the observation of single nanotube spectroscopy for the case of carbon nanotubes (Section 3). We choose the bismuth nanowire and carbon nanotube systems as model systems of nanoscience because they can be understood from a fundamental standpoint and predictions about their properties can be made. Thus bismuth nanowires and carbon nanotubes provide a cornerstone for discussing fundamental principles of nanoscience and for the development of applications based on nanomaterials.

2. Bismuth nanowires

Bismuth provides a very attractive model system for studying low-dimensional physical phenomena because of the very large anisotropy of the three ellipsoidal constant energy surfaces for electrons, their high carrier mobility, and the very light effective masses that can be observed with these carriers. Since bismuth is a semimetal with a very small band overlap energy, the fabrication of nanowires of sufficiently small diameters provides an opportunity to observe a strong dependence of its electronic properties as the nanowire diameter becomes smaller, thereby decreasing its band overlap and decreasing its carrier density. As the wire diameter becomes even smaller, semimetallic bismuth is transformed into a semiconductor below a certain wire diameter (see Fig. 7), depending on the temperature, the crystalline axis of the nanowire, and the amount of antimony that is added to the bismuth. The occurrence of the semimetal–semiconductor transition makes it possible to exploit the highly desirable anisotropic electronic properties of bismuth for new categories of applications that depend on having a new form of bismuth with only electrons or only holes. In addition, bulk bismuth has carriers with very long mean free paths

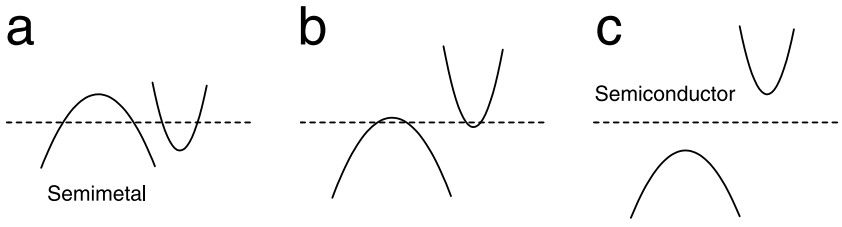

Fig. 7. Schematic diagram of the bismuth nanowire semimetal–semiconductor electronic transition as the lowest conduction subband at the L-point moves up in energy, and the highest valence subband at the T-point moves down in energy as the nanowire diameter d_W decreases. (a) $d_W \gg 50$ nm, (b) $d_W \simeq 50$ nm, (c) $d_W \ll 50$ nm.

which is useful for electronic transport, and heavy mass ions which are highly effective for scattering phonons, making bismuth a very attractive material for thermoelectric applications. Bismuth can also be alloyed isoelectronically with antimony to yield a high mobility alloy, thereby giving much greater flexibility in tailoring the properties of bismuth-related nanowires for specific applications [1].

As a bulk crystalline material, bismuth is semimetallic with an equal number of electrons and holes. This condition makes 30 bismuth undesirable for certain applications, such as thermoelectricity, because of the approximate cancellation between the contributions to the Seebeck coefficient (thermopower) S from the electron ($-$) and hole (+) carriers. It was early recognized that bulk bismuth could, however, be a good thermoelectric material, if the hole carriers could somehow be removed, and bismuth could be made into an n-type semiconductor. It was further found [27] that the addition of antimony could transform bismuth into a semiconductor for a narrow range of antimony concentrations and still maintain a reasonably high carrier mobility.

Low dimensionality offers us an opportunity to transform bismuth from a semimetal to a semiconductor without the addition of antimony (see Fig. 7). As the quantum wire width decreases, the band edge for the lowest subband in the conduction band rises above that for the highest subband in the valence band, thereby inducing a semimetal–semiconductor transition. Since the electronic structure of bulk bismuth is well understood, it has been straightforward to predict the wire diameter below which bismuth nanowires become semiconducting [28]. This value turns out to be on the order of 40–50 nm at 77 K, depending on the crystalline orientation of the nanowires. These nanowire diameters are relatively large and can readily be fabricated in the laboratory by presently available synthesis methods [1].

Arrays of hexagonally packed parallel bismuth nanowires, 7–110 nm in diameter and 25–65 μm in length, have been prepared (see Fig. 8a) [29]. These nanowires are embedded in a dielectric matrix of anodic alumina, which, because of its array of parallel nanochannels, is used as a template for preparing Bi nanowires. Materials science principles serve to confine the bismuth to these nanochannels because the bismuth does not diffuse into the anodic alumina matrix, which forms an excellent barrier material [1]. The Bi nanowires are each highly crystalline (see Figs. 8 and 9) and are highly oriented with a common crystallographic direction along the wire axis, as shown by the X-ray diffraction pattern in Fig. 8b. Since the band structure of Bi is highly anisotropic, the transport properties of Bi nanowires are expected to be dependent on the crystallographic orientation along the wire axes. In addition, structural analysis shows that the crystal structure of bulk Bi is maintained in the nanowires, indicating that many properties of bulk Bi may be utilized in modeling the behavior of Bi nanowires.

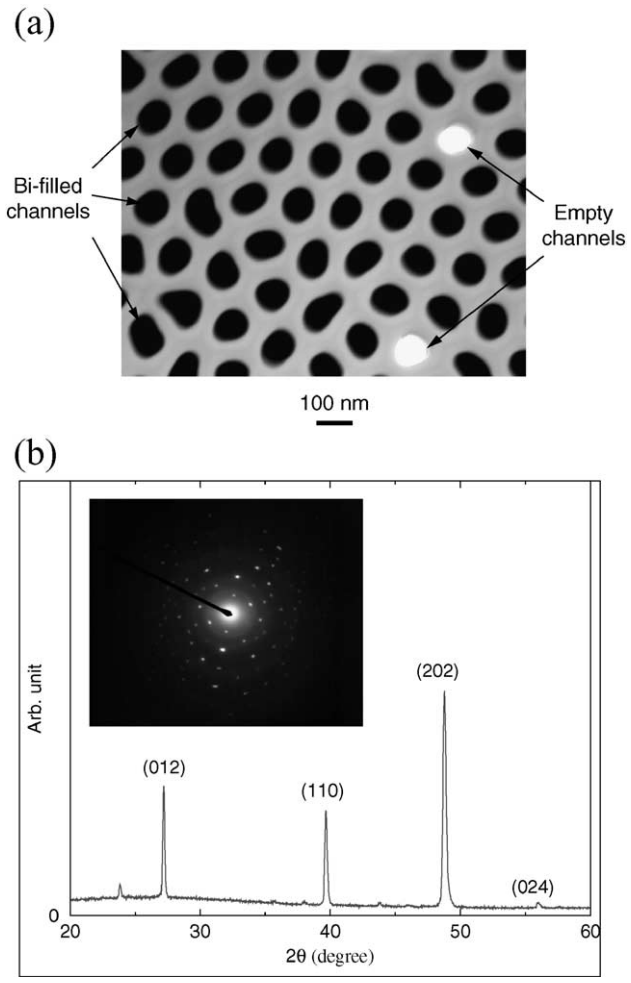

Fig. 8. (a) Cross-sectional view of the cylindrical channels of 65 nm average diameter of an anodic alumina template shown as a transmission electron microscope (TEM) image. The template has been mostly filled with bismuth (dark regions), and the TEM image was taken after the top and bottom sides of the sample had been ion milled with 6 kV Ar ions. (b) X-ray diffraction (XRD) pattern for the anodic alumina/Bi nanowire composites. The average wire diameter of the Bi nanowires is about 52 nm. The inset in the figure shows the selected area electron diffraction (SAED) pattern taken from the same sample. The XRD and SAED experimental results indicate that Bi nanowires are highly crystalline and possess two preferred growth orientations: (101) for d_W>50 nm and (012) for d_W<50 nm [28,29].

To model the electronic structure, we assume, as a first approximation, the simplest possible model for an ideal 1-D quantum wire, where the carriers are confined inside a cylindrical potential well, bounded by a barrier of infinite potential height. An extension of this simple approach provides a reasonable approximation for a Bi nanowire embedded in an alumina template, in view of the large band gap of the anodic alumina template (3.2 eV), which provides excellent carrier confinement for the embedded quantum wires. Due to the small electron effective mass components of Bi, the quantum confinement effects in Bi nanowires are more prominent than for other wires with

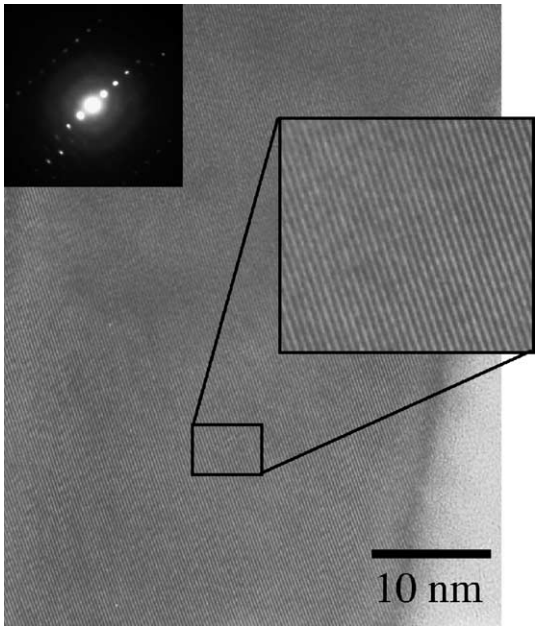

Fig. 9. High resolution TEM lattice image of a bismuth nanowire showing the excellent ordering of the lattice planes. The inset is a selected area diffraction pattern for this nanowire [1].

the same diameter. This model has been used successfully to predict the wire diameter where the semimetal–semiconductor transition occurs as a function of crystallographic orientation and temperature [28].

Measurements of the transport properties of these arrays of Bi nanowires have been carried out for wires of different diameters as a function of temperature and magnetic field, demonstrating the semimetal–semiconducting transition, and showing ballistic transport at low temperature [30]. Good agreement between transport measurements and the modeling calculations has been achieved, thereby validating the use of bismuth nanowires as a model system for studying nanowire structure/property relations. The ability to control the electronic properties over a wide range by alloying with Sb has been shown to be important for selected applications. As mentioned above, alloying provides another parameter in controlling the properties of bismuth-related nanowires. The same basic synthesis methods used for preparing bismuth nanowires can be used to prepare $Bi_{1-x}Sb_x$ alloy nanowires [31]. For example, better thermoelectric performance is predicted for $Bi_{1-x}Sb_x$ alloy nanowires than for pure Bi nanowires of the same diameter [33]. This has recently been verified experimentally by studying the Seebeck coefficient of bismuth and $Bi_{1-x}Sb_x$ nanowires as a function of diameter (keeping the composition constant) and as a function of Sb concentration keeping the nanowire diameter constant [31,32].

Furthermore, Sb alloying is even more important for improving the capabilities for *p*-type bismuth, which has lower mobilities than *n*-type bismuth, in both bulk and nanowire forms [1]. This can be understood by examining the phase diagram of bismuth nanowires as a function of wire diameter and Sb concentration shown in Fig. 10. The semimetal and the indirect semiconductor states in the low antimony content region ($x \leq 0.13$) have the highest valence band extremum at the *T*-point, while those states in the higher antimony content region ($x \geq 0.13$) have their *H*-point hole pockets at the highest energy. Along the solid lines in this "phase diagram", the extrema of the first subband of carrier pockets at two different points in the Brillouin zone coalesce in energy. The bold arrow in the center of the diagram points to the particularly interesting situation where the extrema of all 10 hole pockets coalesce in energy (wire diameter is 60 nm, $x = 0.13$), resulting in a high density of states, which is, for example, beneficial for increasing the magnitude of the Seebeck coefficient. This diagram also predicts a shift to higher values of the critical diameter at which the overlap between the *L*-point electron subbands and the *T*-point hole subbands vanishes (semimetal-to-semiconductor transition) as Sb is added to pure Bi. We therefore expect to obtain higher thermoelectric performance at larger diameters when compared to Bi nanowires. This is confirmed by experimental observation [32]. New physics, arising from the wire diameter and Sb composition dependence of the electronic structure of Bi nanowires, gives rise to the simultaneous confluence [33] of the valence band edge energies for the six *H*-point hole pockets, the three *L*-point hole pockets and the *T*-point hole pocket in *p*-type $Bi_{1-x}Sb_x$ nanowires (see Fig. 10), indicating a new strategy for designing nanostructures to achieve superior thermoelectric properties. The good agreement between transport measurements on $Bi_{1-x}Sb_x$ nanowires and model calculations [31] offers promise that it may be

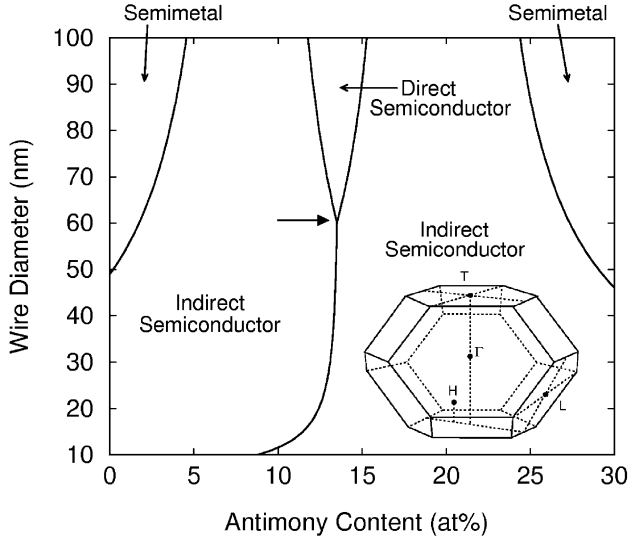

Fig. 10. Phase diagram of the electronic band structure of $Bi_{1-x}Sb_x$ nanowires. The bold arrow in the center of the diagram points at the condition where the 10 hole pockets (about the T-point, the three L-points and the six H-points in the Brillouin zone) coalesce in energy. The locations of these points in the Brillouin zone are shown in the inset [33].

possible to produce both *n*-type and *p*-type nanowire arrays of interest for thermoelectric and many other applications of bismuth nanowires.

In addition to their promise for thermoelectric applications, $Bi_{1-x}Sb_x$ nanowires also constitute an attractive model system to study their transport behavior in low-dimensional structures due to their tunable band structures [35], small electron effective masses, and long carrier mean free paths. Various transport measurements have been performed in conjunction with theoretical models to investigate the unique semimetal-to-semiconductor transition in $Bi_{1-x}Sb_x$ nanowires. Fig. 11 shows the temperature dependence of the resistance for Bi nanowires with various diameters ($7 \le d_W \le 200$ nm) normalized to their resistance at 300 K [34]. The temperature dependence of the resistance ratio of Bi nanowires is very sensitive to the wire diameter due to the semimetal-to-semiconductor transition in Bi-related systems. In Fig. 11, the measured resistance ratio of semimetallic Bi nanowires exhibits a non-monotonic T dependence with a maximum for wire diameters ≥ 70 nm, while the resistance ratios of the smaller diameter nanowire samples that are expected to be semiconducting ($d_W \le 50$ nm) decrease monotonically with increasing T. In addition, the resistance ratio of the semiconducting Bi nanowires ($d_W \le 50$ nm) displays a weaker T dependence as the

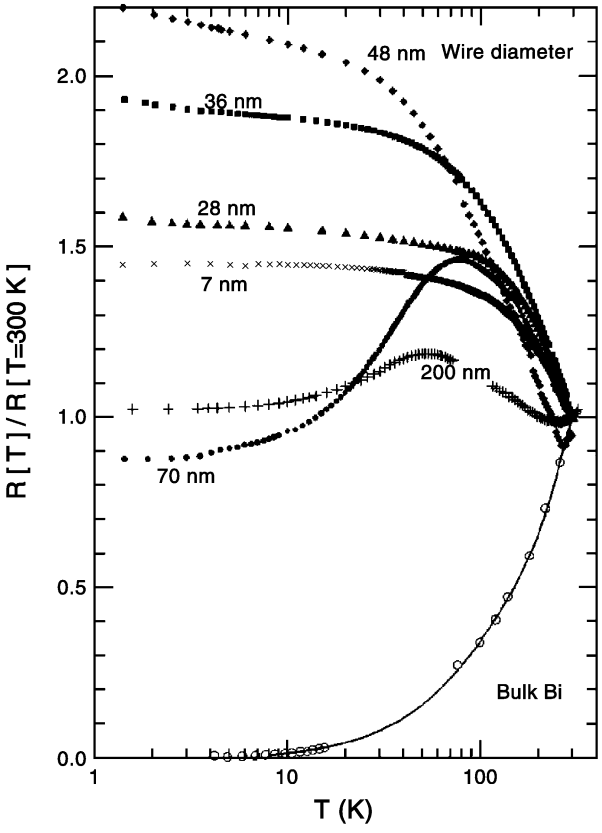

Fig. 11. Measured temperature dependence of the normalized resistance of bulk Bi and Bi nanowires of various wire diameters ($7 \le d_W \le 200$ nm) [30,34].

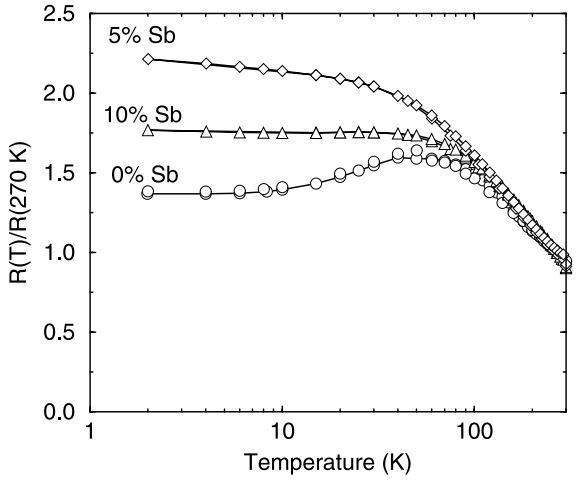

Fig. 12. Measured temperature dependence of the resistance normalized to the resistance at 270 K of 65 nm $Bi_{1-x}Sb_x$ nanowires with different Sb concentrations [32]. Such measurements are used to provide information on the semimetal–semiconductor transition, which occurs at larger wire diameter as a result of Sb addition.

diameter decreases. This non-monotonic shift in the T dependence of the resistance ratio as the wire diameter varies is also observed in the normalized $R(T)$ results of 65 nm $Bi_{1-x}Sb_x$ nanowires of different Sb contents, as shown in Fig. 12, where the measured resistance ratio of pure Bi nanowires ($x = 0$) exhibits a non-monotonic T dependence with a maximum at ~ 70 K, while the resistance ratio of the two alloy nanowire samples (with 5 and 10 at.% Sb) decrease monotonically with increasing T. In addition, the resistance ratio of the $Bi_{0.95}Sb_{0.05}$ nanowires displays a stronger T dependence than that of the $Bi_{0.90}Sb_{0.10}$ nanowires. The resemblance in the two sets of experimental findings both suggests that variation of the temperature dependence of the resistance of $Bi_{1-x}Sb_x$ nanowires is caused by a common effect on the band

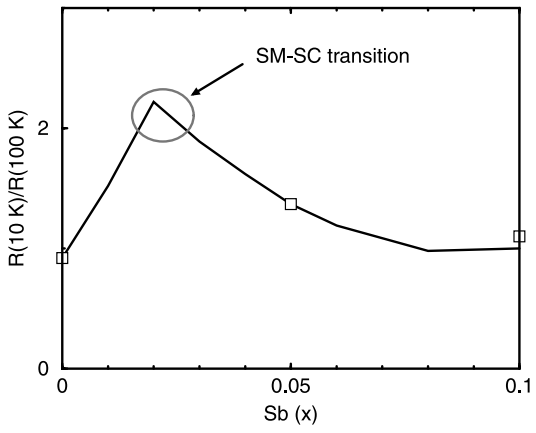

Fig. 13. Predicted values of the resistance ratio $R(10\text{ K})/R(100\text{ K})$ as a function of Sb content in 65 nm $Bi_{1-x}Sb_x$ nanowires [32]. The semimetal–semiconductor transition is expected to occur at the peak in this plot for a given nanowire diameter. The solid curve gives theoretical predictions consistent with the experimental points.

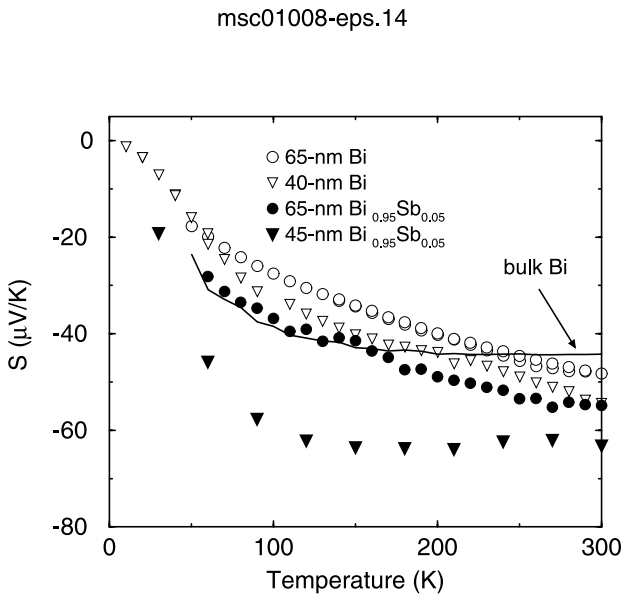

Fig. 14. Measured Seebeck coefficient as a function of temperature for Bi (○, ▽) and $Bi_{0.95}Sb_{0.05}$ (●, ▼) nanowires with different diameters. The solid curve denotes the Seebeck coefficient for bulk Bi [32].

structure and transport properties, i.e. the semimetal-to-semiconductor transition [28]. The resistance ratio R(10 K)/R(100 K) for 65 nm $Bi_{1-x}Sb_x$ nanowires has been calculated as a function of x, and the results for this calculation are also shown in Fig. 13 [32]. We note that as x increases, the resistance ratio of semimetallic wires rises due to the decreased band overlap between the conduction and the valence bands. In contrast, the resistance ratio decreases for semiconducting wires due to the increasing dominance of extrinsic carriers. The maximum in the resistance ratio R(10 K)/R(100 K) at $x \sim 0.02$ corresponds to the Sb content for the predicted semimetal–semiconductor transition. Thus, by examining the resistance ratios of Bi and $Bi_{1-x}Sb_x$ nanowires as a function of wire diameter and x, we can experimentally identify the actual wire diameter and Sb content at which the semimetal–semiconductor transition occurs [32].

The Seebeck coefficient measurements are essential for evaluating the performance of thermoelectric materials. Since the Seebeck coefficient measurement is independent of the number of nanowires contributing to the signal, the measurements on nanowire arrays are in theory as informative as single-wire measurements, and the results, in conjunction with some modeling, can provide valuable information about the Fermi energy and the carrier concentration. Fig. 14 shows the measured Seebeck coefficient as a function of temperature for nanowire arrays with different diameters and Sb contents, confirming that the Seebeck coefficient increases as the wire diameter decreases and the Sb concentration increases, in agreement with theoretical expectations.

The ability to prepare bismuth in semiconductor form through the growth of nanowires with diameters less than 50 nm opens up many new opportunities to study a material with an unusual electronic structure under new conditions, thereby providing new possibilities for interesting applications to nanotechnology.

3. Carbon nanotubes

Carbon nanotubes can be considered as a prototype for 1-D nanotubes because of their relative simplicity, their unique properties, the large amount of information available about them, and their promise for practical applications. There are in fact many types of carbon nanotubes, including single wall carbon nanotubes, double wall carbon nanotubes, multi-wall carbon nanotubes, intercalated nanotubes, and nanotubes filled with various species constituting internal nanowires including fullerenes and even fullerenes filled with metal species (endohedral fullerenes) (see Fig. 15). We focus our attention here on single wall carbon nanotubes because of their simplicity relative to other nanotubes, and

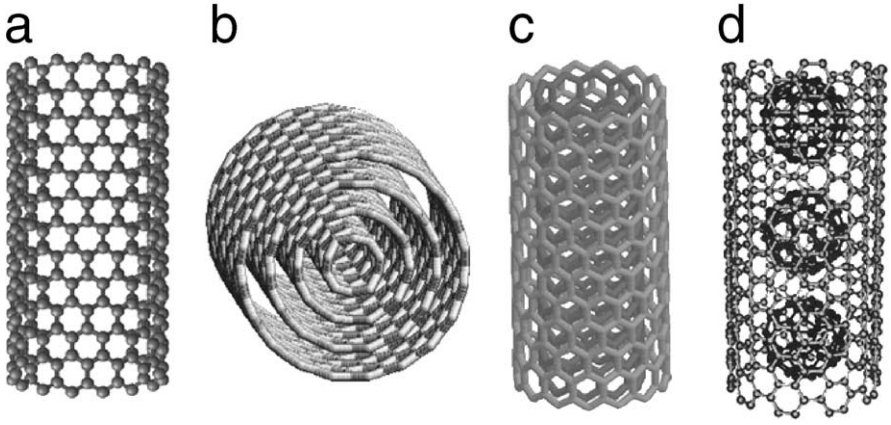

Fig. 15. Schematic diagram of (a) a single wall carbon nanotube (SWNT), (b) a multi-wall carbon nanotube (MWNT), (c) a double wall carbon nanotube (DWNT) and (d) a peapod nanotube consisting of a SWNT filled with fullerenes (e.g., C_{60}).

the high ability for theory to predict nanotube properties based on their structure.

A single wall carbon nanotube (SWNT) can be considered as a single atomic layer of 2-D graphite rolled up into a seamless cylinder. The structure of each nanotube is uniquely described by two integers (n, m), which refer to the number of $\vec{a}_1$ and $\vec{a}_2$ unit vectors of the 2-D graphene lattice that are contained in the chiral vector, $\vec{C}_h = n\vec{a}_1 + m\vec{a}_2$, which spans the circumference of each nanotube [2]. The chiral vector $\vec{C}_h$ together with the translation vector $\vec{T}$ along the nanotube axis and normal to $\vec{C}_h$ define the unit cell of the nanotube [2]. Furthermore, from the (n, m) indices, one can directly determine the nanotube diameter d_t, and the chiral angle θ. We can then calculate for each (n, m) nanotube the electronic energy band structure. The density of electronic states and the electron energy dispersion relations are uniquely determined for each (n, m) nanotube [2,36], as well as the energies of the so-called van Hove singularities in the density of states, where the magnitude of the density of states is very high (see Figs. 1c and 16a). If we keep the nanotube diameter approximately constant and change the chiral angle, we see significant changes in the density of states for the six (n, m) nanotubes shown in Fig. 16a.

It is well established [2] that the (n, m) indices are crucial to the nanotube electronic structure. Most striking is the distinction between metallic and semiconducting nanotubes, namely those SWNTs for which $|n-m| = 3q$ are metallic, and those for which $|n-m| = 3q \pm 1$ are semiconducting, where q is an integer [2,40]. Thus we see that 2/3 of the nanotubes correspond to semiconducting nanotubes and 1/3 to metallic nanotubes. This remarkable property about carbon nanotubes is a quantum mechanical phenomenon based on the special symmetry of 2-D graphite. It has, however, proven difficult to measure (n, m) experimentally and then to carry out property measurements on the same SWNT.

It has recently been shown that the resonance Raman spectra from one isolated nanotube (such as shown in Fig. 17b) can conveniently provide a determination of (n, m). The ability to use resonance Raman spectroscopy to determine the geometrical structure is another remarkable property about carbon nanotubes [43]. Generally speaking, Raman spectroscopy measures phonon frequencies, but under resonance conditions where the phonons and electrons are strongly coupled, this technique can also be used to provide information about the electronic structure. Carbon nanotubes are special materials for which the electronic structure for each nanotube is uniquely determined by its (n, m) indices, and for this reason it is possible to determine the geometrical structure of a single wall carbon nanotube from resonance Raman spectroscopy, as explained below.

The weak dependence of the electronic energy bands of SWNTs on the nanotube chiral angle θ relates to the wave vector k along the nanotube axis and to the three-fold symmetry of the electronic dispersion relations of 2-D graphite about the K-point of the 2-D graphene Brillouin zone (see Fig. 16b), where the graphene (2-D graphite) valence and conduction bands are degenerate, forming a zero band gap semiconductor [2]. Very close to the K-point, the graphene electronic energy bands exhibit circular constant energy contours, but as we move away from the K-point, a trigonal warping effect becomes apparent [37,44], as shown in Fig. 16b. This trigonal warping effect is responsible for the unique spectrum of the singularities in the density of states of the conduction and valence bands for each (n, m) SWNT (Fig. 16a), when the energy bands of the graphene lattice are zone folded to form the energy bands of the SWNTs [2,37]. This chirality dependence stems from the dependence of the direction of the nanotube axis on the (n, m) indices, thus leading to one-dimensional lines cutting the constant energy contours differently, depending on the

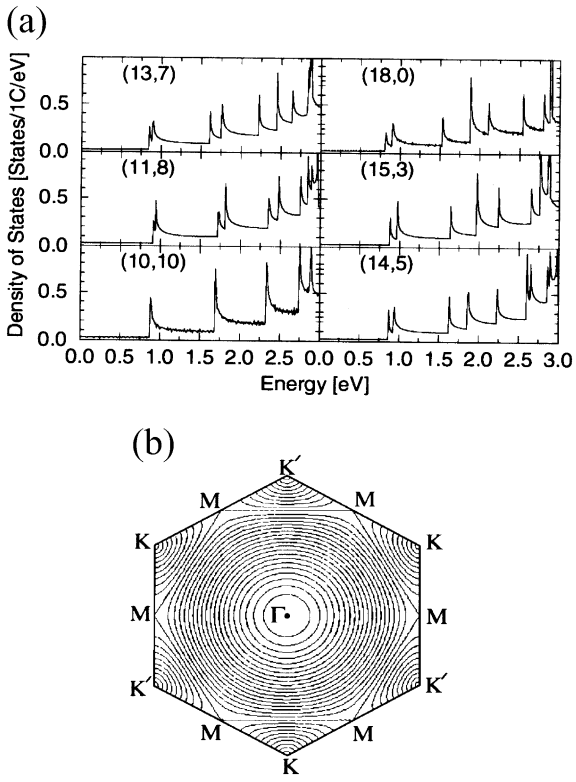

Fig. 16. (a) The 1-D electronic density of states vs. energy E (plotted from the Fermi level $E=0$) for several metallic nanotubes of approximately the same diameter, showing the effect of chirality and trigonal warping (see text) on the van Hove singularities in the density of states: (10, 10) (armchair), (11, 8), (13, 7), (14, 5), (15, 3) and (18, 0) (zigzag). Only the densities of states for the conduction π^* band are shown; the mirror image of these plots gives the electronic density of states for the valence π band [37,38]. The calculations are based on the tight binding approximation, assuming the energy overlap integral is $\gamma_0 = 2.9$ eV and the wave function overlap integral vanishes $s=0$ [2]. (b) Plot of the 2-D equi-energy contours of 2-D graphite, showing trigonal warping effects in the contours, as we move from the K-point in the $K-\Gamma$ or $K-M$ directions. The equi-energy contours are circles near the K-point and near the center of the Brillouin zone. But near the M-points on the zone boundary, the contours are straight lines, which connect the nearest M-points [37,39].

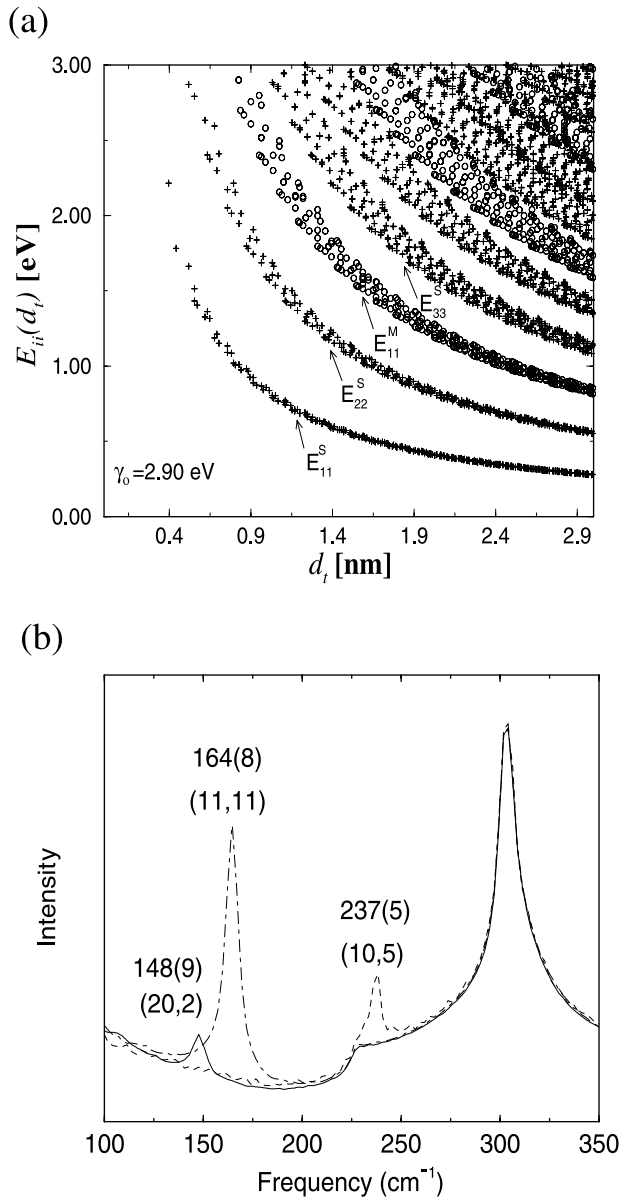

Fig. 17. (a) Calculated [41] energy separations E_{ii} between van Hove singularities i in the 1-D electronic density of states of the conduction and valence bands for all (n, m) values vs. nanotube diameter $0.4 \le d_t \le 3.0$ nm, using a value for the carbon–carbon energy overlap integral of $\gamma_0 = 2.9$ eV and a nearest neighbor carbon–carbon distance $a_{C-C} = 1.42$ Å [37,42]. Semiconducting (S) and metallic (M) nanotubes are indicated by crosses and open circles, respectively. The index i in the interband transitions E_{ii} denotes a particular transition between the van Hove singularities, with $i = 1$ being closest to the Fermi level taken at $E = 0$. The superscripts M and S on E_{ii} denote the interband transition energies for metallic and semiconducting tubes, respectively. (b) The three Raman spectra (solid, dashed, and dash-dotted curves) were taken at three different spots on the Si substrate, showing the presence of only one resonant nanotube and one RBM frequency for each of the three laser spots. The RBM frequencies (widths) and the (n, m) assignments for each resonant SWNT are displayed. The 303 cm^{-1} feature comes from the Si substrate and is used for calibration of the SWNT spectra [43].

(n, m) indices. The existence of the band degeneracy at the K-point and the presence of trigonal warping effects in graphite are phenomena based on symmetry considerations, and are not related to the method used for calculations of the electronic structure.

Since the peak energies in the density of states are unique for each pair of (n, m) integers, the interband transition energies E_{ii} between the ith singularities in the valence and conduction bands are also unique. Here the integer i denotes a particular singularity in the joint density of states (JDOS) and i increases as the magnitude of the energy E_{ii} increases relative to the Fermi level E_F. A plot of all the E_{ii} where the singularities in the JDOS occur is presented in Fig. 17a as a function of nanotube diameter d_t in the range $0.4 \le d_t \le 3.0$ nm [41]. From the above discussion, we conclude that each nanotube (n, m) has a unique set of interband energies E_{ii} denoting the energy differences between the ith van Hove singularities in the conduction and valence bands. And, conversely, if one interband energy E_{ii} and a nanotube diameter d_t are specified (Fig. 17a), then its corresponding unique (n, m) can in general be identified from this plot.

A large enhancement in the Raman signal occurs in the resonance Raman effect, when the incident or scattered photon is in resonance with a singularity in the 1-D joint density of states (JDOS) of the SWNT. This large enhancement allows the observation of a well-resolved Raman signal from an individual SWNT as shown in Fig. 17b. This figure shows three Raman spectra in the low frequency radial breathing mode region, taken for three different isolated SWNTs, each within a different light spot, about 1 μm in diameter, on a sample of isolated SWNTs. It is noteworthy that the intensity of the Raman signal from a strongly resonant tube, such as the (11, 11) SWNT in Fig. 17b, is comparable to that from the Si substrate, even though the SWNT signal comes from only a small fraction of the number of C atoms relative to the number of substrate Si atoms (C/Si ~ 10^{-6}) within the optical beam. This high sensitivity for SWNTs in resonance with the incident photon is the basis for the ability to observe a Raman spectrum from a single nanotube [43].

We now summarize the necessary ingredients for carrying out a (n, m) determination from the measured resonance Raman spectra. From the experiment, the radial breathing mode frequency, where all the atoms are vibrating in phase in the radial direction, ω_{RBM}, is used to obtain the nanotube diameter according to the relation [2,45]

$$\omega_{RBM} = \alpha/d_t \quad (1)$$

and α has been experimentally found to be 248 ± 8 cm^{-1} nm for isolated SWNTs on an oxidized silicon substrate. In addition to d_t, it is necessary to have an experimental value for E_{ii} in order to determine (n, m) from Fig. 17a. The evaluation of E_{ii} can be carried out in various ways and to various degrees of accuracy, but the important concern is to use sufficient accuracy to be able to distinguish d_t and E_{ii}

values of a given (n, m) tube from those of another (n' , m') tube.

The determination of E_{ii} can, in principle, be carried out simply by using a tunable laser to bring E_{laser} into perfect resonance with E_{ii}, where the maximum intensity in the Raman spectrum occurs at $E_{ii} = E_{laser}$ or at $E_{ii} = E_{laser} \pm E_{phonon}$. In practice, such a tunable laser system is not yet available as a standard laboratory tool. One method that is readily available to determine the magnitude of E_{ii} directly requires measurement of both the radial breathing mode spectra for the Stokes (phonon emission) and anti-Stokes (phonon absorption) processes [46,47]. This procedure is very sensitive to E_{ii} even when the ω_{RBM} values for two or more SWNTs are very close to each other. In this method, the ratio of the anti-Stokes to Stokes intensities $I_{AS} \neq I_S$ for the radial breathing modes is measured. This ratio is found to be very sensitive to the energy difference between E_{ii} and E_{laser} and can thus be used to determine the magnitude of E_{ii} to 10 meV accuracy [46,47].

The E_{ii} determination for an isolated nanotube can be even more simply carried out by using a single laser excitation energy E_{laser} when the nanotube is in approximate resonance with E_{laser} by: (1) measuring the intensity of the radial breathing mode, (2) calculating the E_{ii} values of various candidate (n, m) nanotubes with similar d_t values as determined by the frequency of the radial breathing mode, and (3) then making a comparison between the relative RBM intensities of the test SWNT with the intensities of other SWNTs whose (n, m) indices have previously been determined. When this very simple method is used for the (n, m) identification, the tentative (n, m) assignment is checked by considering the characteristics of the other features in the Raman spectra that are sensitive to (n, m) [48]. If the (n, m) values of every nanotube in the sample must be found, then a tunable laser is needed to provide a resonant excitation energy for each nanotube, so that a complete (n, m) Raman characterization can be carried out for each SWNT. The use of a tunable laser is also useful for an experimental determination of the profile of the van Hove singularity [49].

The determination of the geometrical structure of a nanotube can be combined with other measurement techniques to explore many physical properties at the single nanotube level as a function of the nanotube diameter and chirality. In this way, many fundamental aspects about the physical properties of nanotubes should be illuminated at the single nanotube level in the near future.

Acknowledgements

The support from MURI subcontract 0205-G-7A114-01, NSF Grant DMR-01-16042, and US Navy Contracts N00167-98-K0024 and N66001-00-1-8603, and ONR N00014-02-1-0865 are gratefully acknowledged. The Brazilian authors (AJ, AGSF, MAP) acknowledge support from CNPq-Brazil, especially Grant CNPq 910120/99-4, and from the Instituto do Milenio de Nanociencias. RS acknowledges a Grant-in-Aid (No. 13440091) from the Ministry of Education, Japan. The authors would like to thank G. Chen, T.C. Harman, J.P. Issi, John Stockholm, P.C. Eklund and K.L. Wang for their valuable discussions.

References

[1] M.S. Dresselhaus, Y.-M. Lin, T. Koga, S.B. Cronin, O. Rabin, M.R. Black, G. Dresselhaus, Low dimensional thermoelectricity, in: T.M. Tritt (Ed.), Semiconductors and Semimetals: Recent Trends in Thermoelectric Materials Research III, vol. 71, Academic Press, San Diego, CA, 2001, pp. 1–121, Chap. 1.

[2] R. Saito, G. Dresselhaus, M.S. Dresselhaus, Physical Properties of Carbon Nanotubes, Imperial College Press, London, 1998.

[3] R. Tenne, A.K. Zettl, Nanotubes from inorganic materials, in: M.S. Dresselhaus, G. Dresselhaus, P. Avouris (Eds.), Carbon Nanotubes: Synthesis, Structure, Properties and Applications, Springer Series Topics in Applied Physics, vol. 80, Springer-Verlag, Berlin, 2001, pp. 81–112.

[4] G.L. Frey, R. Tenne, M.J. Matthews, M.S. Dresselhaus, G. Dresselhaus, Optical properties of MS_2 (M = Mo, W) inorganic fullerene-like and nanotube material optical absorption and resonant Raman measurements, J. Mater. Res. 13 (1998) 2412–2417.

[5] R. Tenne, L. Margulis, M. Genut, G. Hodes, Polyhedral and cylindrical structures of WS_2, Nature (Lond.) 360 (1992) 444–445.

[6] G.L. Frey, S. Ilani, M. Homyonfer, Y. Feldman, R. Tenne, Optical-absorption spectra of inorganic fullerene-like MS_2 (M = Mo, W), Phys. Rev., B 57 (1998) 6666–6671.

[7] A.M. Morales, C.M. Lieber, A laser ablatin method for the synthesis of crystalline semiconductor nanowires, Science 279 (1998) 208.

[8] D. Xu, D. Chen, Y. Xu, X. Shi, G. Guo, L. Gui, Y. Tang, Preparation of ii–vi group semiconductor nanowire arrays by dc electrochemical deposition in porous aluminum oxide templates, Pure Appl. Chem. 72 (2000) 127.

[9] D. Xu, Y. Xu, D. Chen, G. Guo, L. Gui, Y. Tang, Preparation of cds single-crystal nanowires by electrochemically induced deposition, Adv. Mater. 12 (2000) 520.

[10] X. Duan, J. Wang, C.M. Lieber, Synthesis and optical properties of gallium arsenide nanowires, Appl. Phys. Lett. 76 (2000) 1116.

[11] X. Duan, C.M. Lieber, General synthesis of compound semiconductor nanowires, Adv. Mater. 12 (2000) 298.

[12] X. Sun, The effect of quantum confinement on the thermoelectric figure of merit, PhD thesis, Massachusetts Institute of Technology, Department of Physics (June 1999).

[13] R. Ferre, K. Ounadjela, J.M. George, L. Piraux, S. Dubois, Magnetization processes in nickel and cobalt electrodeposited nanowires, Phys. Rev., B 56 (1997) 14066.

[14] G.H. Zeng, A. Shakouri, C. La Bounty, G. Robinson, E. Croke, P. Abraham, X.F. Fan, H. Reese, J.E. Bowers, Si-Ge micro-cooler, Electron. Lett. 35 (1999) 2146–2147.

[15] Y. Li, J. Wang, Z. Deng, Y. Wu, X. Sun, D. Yu, P. Yang, Bismuth nanotubes: a rational low-temperature synthetic route, J. Am. Chem. Soc. 123 (2001) 9904–9905.

[16] K. Miki, J.H.G. Owen, D.R. Bowler, G.A.D. Briggs, K. Sakamoto, Bismuth-induced structures on Si (001) surfaces, Surf. Sci. 421 (1999) 397–418.

[17] M.H. Huang, S. Mao, H. Feick, H. Yan, Y. Wu, H. Kind, E. Weber, R. Russo, P. Yang, Room-temperature ultraviolet nanowire nanolasers, Science 292 (2001) 1897.

[18] M.S. Gudiksen, C.M. Lieber, Diameter-selective synthesis of semiconductor nanowires, J. Am. Chem. Soc. 122 (2000) 8801–8802.

[19] C.M. Lieber, The incredible shrinking circuit, Sci. Am. 285 (2001) 50–56.
[20] J. Wang, M.S. Gudiksen, X. Duan, Y. Cui, C.M. Lieber, Highly polarized photoluminescence and photodetection from single indium phosphide nanowires, Science 293 (2001) 1455–1457.
[21] J.C. Johnson, H. Yan, R.D. Schaller, R.D. Schaller, L.H. Haber, R.J. Saykally, P. Yang, Single nanowire lasers, J. Phys. Chem., B 105 (2001) 11387.
[22] Y. Wu, F.R.J. Wang, Block-by-block growth of single-crystalline Si/SiGe superlattice nanowire, Nano Lett. 2 (2002) 83–86.
[23] M.S. Gudiksen, L.J. Lauhon, J. Wang, D.C. Smith, C.M. Lieber, Growth of nanowire superlattice structures for nanoscale photonics and electronics, Nature (Lond.) 415 (2002) 617–620.
[24] M.T. Björk, B.J. Ohlsson, T. Sass, A.I. Persson, C. Thelander, M.H. Magnusson, K. Deppert, L.R. Wallenberg, L. Samuelson, One-dimensional steeplechase for electrons realized, Nano Lett. 2 (2002) 87–89.
[25] Y.-M. Lin, unpublished (2002).
[26] Y.-M. Lin, O. Rabin, M.S. Dresselhaus, Segmented nanowires: a theoretical study of thermoelectrics, Long Beach, CA, 2002 (in press).
[27] A.L. Jain, Temperature dependence of the electrical properties of bismuth–antimony alloys, Phys. Rev. 114 (1959) 1518.
[28] Y.M. Lin, X. Sun, M.S. Dresselhaus, Theoretical investigation of thermoelectric transport properties of cylindrical Bi nanowires, Phys. Rev., B 62 (2000) 4610–4623.
[29] Z. Zhang, J.Y. Ying, M.S. Dresselhaus, Bismuth quantum-wire arrays fabricated by a vacuum melting and pressure injection process, J. Mater. Res. 13 (1998) 1745–1748.
[30] Y.-M. Lin, S.B. Cronin, J.Y. Ying, M.S. Dresselhaus, J.P. Heremans, Transport properties of Bi nanowire arrays, Appl. Phys. Lett. 76 (2000) 3944–3946.
[31] Y.-M. Lin, S.B. Cronin, O. Rabin, J.Y. Ying, M.S. Dresselhaus, Transport properties of $Bi_{1-x}Sb_x$ alloy nanowires synthesized by pressure injection, Appl. Phys. Lett. 79 (2001) 677–679.
[32] Y.-M. Lin, O. Rabin, S.B. Cronin, J.Y. Ying, M.S. Dresselhaus, Semimetal–semiconductor transition in $Bi_{1-x}Sb_x$ alloy nanowires and their thermoelectric properties, Appl. Phys. Lett. 81 (2002) 2403–2405.
[33] O. Rabin, Y.-M. Lin, M.S. Dresselhaus, Anomalously high thermoelectric figure of merit in $Bi_{1-x}Sb_x$ nanowires by carrier pocket alignment, Appl. Phys. Lett. 79 (2001) 81–83.
[34] J. Heremans, C.M. Thrush, Y.-M. Lin, S. Cronin, Z. Zhang, M.S. Dresselhaus, J.F. Mansfield, Bismuth nanowire arrays: synthesis and galvanomagnetic properties, Phys. Rev., B 61 (2000) 2921–2930.
[35] B. Lenoir, M. Cassart, J.P. Michenaud, H. Scherrer, S. Scherrer, Transport properties of Bi-rich Bi–Sb alloys, J. Phys. Chem. Solids 57 (1996) 89–99.
[36] M.S. Dresselhaus, G. Dresselhaus, P. Avouris, Carbon nanotubes: synthesis, structure, properties and applications, in: Springer Series Topics in Applied Physics, vol. 80, Springer-Verlag, Berlin, 2001, pp. 1–447.
[37] R. Saito, G. Dresselhaus, M.S. Dresselhaus, Trigonal warping effect of carbon nanotubes, Phys. Rev., B 61 (2000) 2981–2990.
[38] R. Saito, H. Kataura, in: M.S. Dresselhaus, G. Dresselhaus, P. Avouris (Eds.), Carbon Nanotubes: Synthesis, Structure, Properties and Applications, Springer Series Topics in Applied Physics, vol. 80, Springer-Verlag, Berlin, 2001, pp. 213–246.
[39] T.W. Odom, J.L. Huang, P. Kim, C.M. Lieber, Atomic structure and electronic properties of single-walled carbon nanotubes, Nature (Lond.) 391 (1998) 62–64.
[40] M.S. Dresselhaus, G. Dresselhaus, P.C. Eklund, Science of Fullerenes and Carbon Nanotubes, Academic Press, New York, NY, 1996.
[41] H. Kataura, Y. Kumazawa, Y. Maniwa, I. Umezu, S. Suzuki, Y. Ohtsuka, Y. Achiba, Optical properties of single-wall carbon nanotubes, Synth. Met. 103 (1999) 2555–2558.
[42] G. Dresselhaus, M.A. Pimenta, R. Saito, J.-C. Charlier, S.D.M. Brown, P. Corio, A. Marucci, M.S. Dresselhaus, On the $\pi-\pi$ overlap energy in carbon nanotubes, in: D. Tománek, R.J. Enbody (Eds.), Science and Applications of Nanotubes, Proceedings of the International Workshop on the Science and Applications of Nanotubes, Michigan State University, East Lansing, MI, USA, July 24–27, 1999, Kluwer Academic Publishing, New York, 2000, pp. 275–295.
[43] A. Jorio, R. Saito, J.H. Hafner, C.M. Lieber, M. Hunter, T. McClure, G. Dresselhaus, M.S. Dresselhaus, Structural (n, m) determination of isolated single-wall carbon nanotubes by resonant Raman scattering, Phys. Rev. Lett. 86 (2001) 1118–1121.
[44] R. Saito, A. Jorio, J.H. Hafner, C.M. Lieber, M. Hunter, T. McClure, G. Dresselhaus, M.S. Dresselhaus, Chirality-dependent G-band Raman intensity of carbon nanotubes, Phys. Rev., B 64 (2001) 85312–85319.
[45] M.S. Dresselhaus, P.C. Eklund, Phonons in carbon nanotubes, Adv. Phys. 49 (2000) 705–814.
[46] A.G. Souza Filho, A. Jorio, J.H. Hafner, C.M. Lieber, R. Saito, M.A. Pimenta, G. Dresselhaus, M.S. Dresselhaus, Electronic transition energy E_{ii} for an isolated (n, m) single-wall carbon nanotube obtained by anti-stokes/stokes resonant Raman intensity ratio, Phys. Rev., B 63 (2001) 241404R.
[47] Z. Yu, L.E. Brus, (n, m) Structural assignments and chirality dependence in single-wall carbon nanotube Raman scattering, J. Phys. Chem., B 105 (2001) 6831–6837.
[48] M.S. Dresselhaus, G. Dresselhaus, A. Jorio, A.G. Souza Filho, R. Saito, Raman spectroscopy of isolated single wall carbon nanotubes, Carbon 40 (2002) 2043–2061.
[49] A. Jorio, A.G. Souza Filho, G. Dresselhaus, M.S. Dresselhaus, R. Saito, J.H. Hafner, C.M. Lieber, F.M. Matinaga, M.S.S. Dantas, M.A. Pimenta, Joint density of electronic states for one isolated single-wall carbon nanotube studied by resonant Raman scattering, Phys. Rev., B 63 (2001) 245416-1–245416-4.